Design Optimization of a Self-circulated Hydrogen Cooling System for a PM Wind Generator Based on Taguchi Method

Gaojia Zhu, *Member, IEEE*, Yunhao Li, and Longnv Li, *Member, IEEE*

***Abstract*—With the continuous improvement of permanent magnet (PM) wind generators' capacity and power density, the design of reasonable and efficient cooling structures has become a focus. This paper proposes a fully enclosed self-circulating hydrogen cooling structure for a originally forced-air-cooled direct-drive PM wind generator. The proposed hydrogen cooling system uses the rotor panel supports that hold the rotor core as the radial blades, and the hydrogen flow is driven by the rotating plates to flow through the axial and radial vents to realize the efficient cooling of the generator. According to the structural parameters of the cooling system, the Taguchi method is used to decouple the structural variables. The influence of the size of each cooling structure on the heat dissipation characteristic is analyzed, and the appropriate cooling structure scheme is determined.**

***Index Terms*—Permanent magnet wind generator, Hydrogen cooling, Taguchi method, Fluidic-thermal coupled fields.**

I. Introduction

WIND energy is nowadays one of the mainstream renewable energy sources worldwide, making significant contributions to the reduction of ever-increasing carbon emissions [1]-[2]. Permanent magnet (PM) generators have been widely used in wind power generation systems because of their high efficiency and high power density [3]-[4], making megawatt (MW)-class direct-drive PM wind generators a hot topic [5].

However, due to the relatively harsh working conditions of wind generators, the heat generation problem is becoming more and more prominent with the continuous increase in the stand-alone capacity of PM wind generators, which poses substantial threats to their working reliability [6]-[7]. Therefore, designing a reasonable cooling system and improving the heat dissipation performance of the machine is of great significance for the safe and stable operation of wind turbines [8].

Manuscript received March 15, 2024; revised May 02, and May 15, 2024; accepted May 24, 2024. Date of publication June 25, 2024; Date of current version June 06, 2024.

This work was supported in part by the "Chunhui Plan" Collaborative Research Project of Chinese Ministry of Education under Grant HZKY20220604, and also by the National Natural Science Foundation of China under Grant 52107007 (*Corresponding Author*: *Longnv Li*)

G. J. Zhu, Y. H. Li, and L. N. Li are with School of Electrical Engineering, Tiangong University, Tianjin 300387, China (e-mail: zhugaojia@tiangong.edu.cn).

Digital Object Identifier 10.30941/CESTEMS.2024.00024

The internal temperature field of a generator is closely related to the fluid field, and the distribution of the fluid field is mainly determined by the cooling system's structures and the coolant's flow states. Consequently, the rational design of the cooling system is the key issue to the design and development of a PM wind generator [9]. [10] proposed a stator channelized water cooling scheme for a 3.2 MW modular PM direct-drive generator. The cooling efficiency is proved superior via numerical simulations. [11] proposed the optimal cooling structure by changing the size of the radial ventilation trench of a 2.5 MW PM generator and comparing the performance of different structural schemes. [12] numerically investigated the heat dissipation capacity of a radially-forced air-cooled fractional slot centrally wound PM wind generator. The fluid flow and temperature fields with different cooling channel numbers and widths are determined. In [13], the computational fluid dynamics (CFD) simulations on the cooling effectiveness of an 8 MW external rotor direct-driven PM wind generator were presented. In [14], the relationship between the air movement in the ventilation duct and the surface heat transfer coefficient was analyzed for a 150 MW air-cooled generator. [15] investigated the spatial fluid flow distributions of the coolant in a generator.

In this paper, based on a 1.65 MW direct-drive PM wind generator, the CFD analysis with the original forced-air-cooled structure is carried out. The calculated temperature rise is compared with the experimental tested values to validate the effectiveness of the simulations. However, the forced-air open-structure cooling system can quickly bring and accelerate dust into the generator, threatening the long-term operation reliability and increasing the maintenance costs. To solve this issue while maintaining the cooling capacity, an enclosed self-circulating hydrogen cooling system is proposed, driving the cooling hydrogen flow by the rotor panel supports as the centrifugal fan. The simulation results prove that it has better heat dissipation performance when compared with that using air as the coolant. The cooling structural parameters of the hydrogen cooling system are then optimized through the Taguchi method.

II. Basic Parameters and Ventilation Structure

A. Basic Parameters of the Generator

The stator of the PM synchronous wind generator has 156

rectangular slots, and rectangular cross-section forming windings are installed in the slots. The rotor section consists of 32 modular poles (16 pairs) sets. The basic parameters are shown in Table I.

TABLE I
BASIC PARAMETERS OF THE PM GENERATOR

Parameter	Value
Magnetic flux/MW	1.65
Rated speed/(r/min)	150
Output voltage/V	690
Rated efficiency/(%)	96.5
Number of pole pairs/ Number of slots	16/156
Inner and outer diameters of the stator/mm	1900, 2110
Inner and outer diameters of the rotor/mm	1735, 1894
PM width	152
Axial length	645
Insulation rating	F
PM material	NdFeB(N40UH)
Silicon steel sheet grade	50DW310

B. The Original Forced-air-cooled Ventilation Structure

The original ventilation system of the 1.65 MW PM wind generator adopts a single-channel axial one, as shown in Fig. 1. A hood is mounted outside the generator, with a partition separates the cold and hot air. Two centrifugal fans are fixed at the upper end of the hood to drive cooling air to the generator. The cooling air flow is illustrated in Fig. 1.

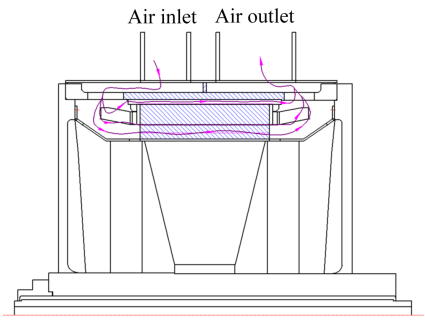

Fig. 1. Original ventilation structure of the PM generator.

III. FORCED AIR-COOLED STRUCTURE ANALYSIS OF PM WIND GENERATORS

A. Mathematical Models

In this paper, the three-dimensional steady-state governing equation of the fluidic-thermal fields in anisotropic media can be expressed as [16]:

$$\frac{\partial}{\partial x}\left(\lambda_x \frac{\partial T}{\partial x}\right)+\frac{\partial}{\partial y}\left(\lambda_y \frac{\partial T}{\partial y}\right)+\frac{\partial}{\partial z}\left(\lambda_z \frac{\partial T}{\partial z}\right)=-q_v \quad (1)$$

where T is the temperature rise, K; λ_x, λ_y, and λ_z are the thermal conductivity along the x, y, and z axes, respectively, W/(m·K); and q_v is the total heat source value, W/m^3.

The laws of mass conservation, momentum, and energy constrain the flow of the coolant in the generator. When the internal fluid flow state of the generator is stable, the general governing equation of the fluid in the Cartesian coordinate system can be expressed as [17]-[18]:

$$\operatorname{div}(\rho u\varphi)=\operatorname{div}(\Gamma \operatorname{grad}\varphi)+S \quad (2)$$

where φ is the general variable; ρ is the fluid density, kg/m^3; Γ is the expansion coefficient; and S is the source term.

B. Basic Assumptions

During calculations, the following assumptions are made according to the structure of the generator and the characteristics of the fluid [19]-[21]:

1) The air is highly turbulent with large Reynolds numbers, therefore, the standard κ-ε model is used in the calculations.

2) The generator is in a stable working state, and the cooling air in the inner air path is continuous, stable, and enclosed.

3) The airflow velocity is much smaller than the wind speed; that is, the Mach number (Ma) is small, which is an incompressible fluid.

4) The insulation and air in the tank are equivalent to the insulating entity wrapped in copper strips.

5) The extension part of the end of the winding is equivalent to a straight conductor of equal length and insulation.

C. Physical Model

The overall model of the generator is complex, to reduce the amount of calculation, a 1/4 calculation model based on the symmetry property is used. The solution domain model is shown in Fig. 2. During calculations, the experimentally tested losses are divided based on the proportion obtained by electromagnetic simulations, and the related heat sources are tabulated in Table II [22]. Among them, the bearing friction loss is obtained from an empirical formula [23]:

$$q_{br}=0.7725\times10^{-3}G_r D_{sh}\omega \quad (3)$$

where G_r is the rotor weight, kg; D_{sh} is the generator shaft diameter, m; and ω is the generator speed, r/min.

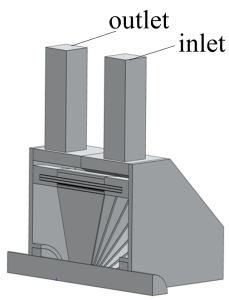

Fig. 2. Calculation model.

TABLE II
GENERATOR LOSS

Parameters	Loss/kW	Loss density /(10^4 W/m^3)
Winding	24.3	17.8
Stator teeth	6.89	3.31
Stator yoke	6.45	2.55
Rotor	1.93	2.56
PM	2.17	3.13
Bearing	0.069	0.47

D. Comparison of Simulation Calculations and Experiments

Fig. 2 shows the fluid-thermal coupling field solution of the

computational model. The overall temperature rise distribution of the generator under the forced air-cooled structure is shown in Fig. 3, and the maximum temperature rise is 72.53 K. From Fig. 4, it can be seen that the highest temperature rise of the generator occurs in the middle of the winding near the outlet. In addition, it can be seen that the temperature rise is lower at the position where the windings deviate from the air inlet. Due to the cooling effect of the internal air, the temperature rise of the end-windings is lower than that of the slot-windings.

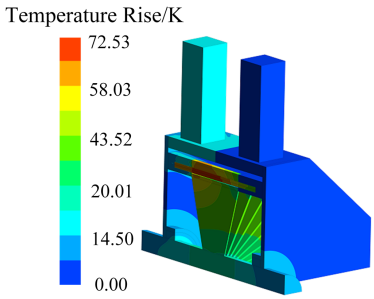

Fig. 3. Overall temperature rise.

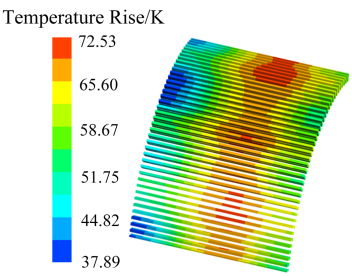

Fig. 4. Winding temperature rise.

Due to the harmonic-introduced eddy-current losses in the PMs and the rotor core, the PMs can generate a temperature rise, as shown in Fig. 5. As can be found from the figure, the cooling effect of the ventilated air in the radial vents, the PM temperature rise distribution also shows an uneven trend. The highest PM temperature rise occurs near the air outlet side. Table III compares the calculated and experimental tested temperature rises of the generator, and the error is small, which verifies the correctness of the mathematical and physical models.

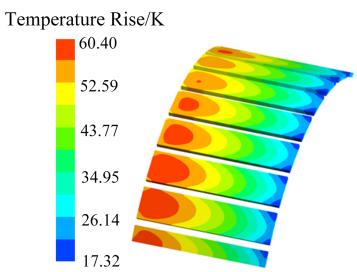

Fig. 5. Temperature rise of PM.

TABLE III
COMPARISON OF SIMULATION RESULTS WITH EXPERIMENTAL VALUES OF TEMPERATURE RISE

Parameters	Simulated Temperature Rise/K	Tested Temperature Rise/K	Error (%)
Windings	72.53	77.7	6.71
PMs	60.40	65.5	7.78

IV. PM WIND GENERATOR ENCLOSED SELF-CIRCULATING HYDROGEN-COOLED STRUCTURE

A. Design and Theoretical Analysis of Cooling Structure

With the forced air-cooling structure, the weight and the mounting space of the PM generator are relatively large due to the external air blowers. In addition, the maintenance costs can also be high as external dust can be brought into the generator together with the external cooling air. Based on the original structure of the PM wind generator, an enclosed self-circulating hydrogen cooling system is designed with the rotor panel supports as the centrifugal blades, as shown in Fig. 6, to drive the cooling hydrogen flow.

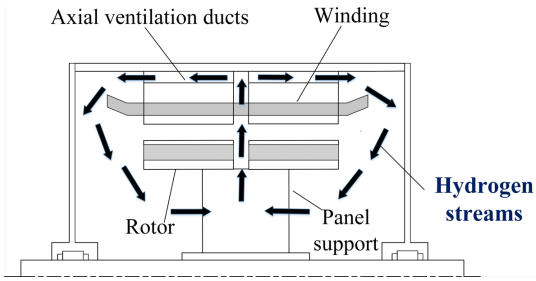

Fig. 6. Enclosed self-circulating hydrogen cooling system.

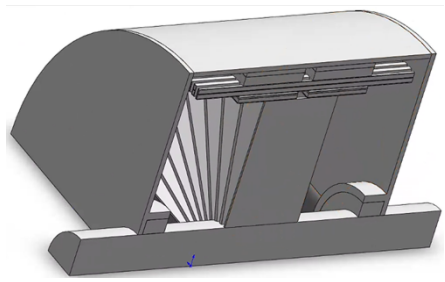

Fig. 7. Calculation model of enclosed self-circulating hydrogen cooling system.

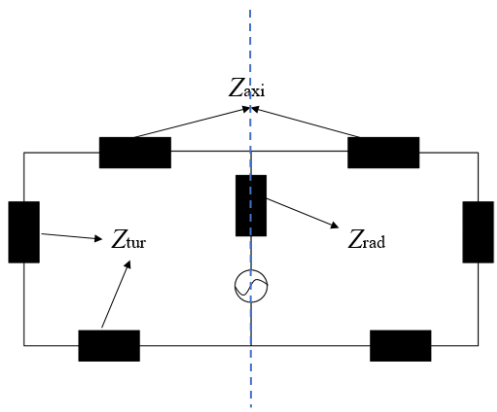

Fig. 8. Illustration on the fluid flow network.

As shown in Fig. 6, the panel-support plates provide air pressure in the radial vents, driving the coolant to flow through the radial air duct opened in the center of the stator and rotor. Then the coolant flows into the generator end cavity through the axial ventilation channels between the stator yoke and the casing, blows the end-windings, and dissipates the heat from them. Although the rotation speed of the generator is low (150 r/min), as the radial diameter of the plate is large,

the linear velocity at the edge of the plate can reach 14.37 m/s, and the cooling system can therefore provide sufficient cooling flow. Fig. 7 shows the numerical calculation model of the flow-thermal coupling field of the enclosed self-circulating cooling system.

The closed self-circulating cooling structure is a hybrid ventilation cooling structure that includes radial ventilation ducts and axial ventilation ducts, with the fluid flow network shown in Fig. 8. In the figure, Z_{rad} is the radial air channel wind resistance, Z_{axi} is the axial air channel wind resistance, and Z_{tur} is the turning wind resistance. The total flow resistance can therefore be modeled by:

$$Z_{total} = \frac{Z_{rad} + \left(Z_{axi} / 24^2 + Z_{tur}\right)}{2^2} = 172.35\ (\mathrm{N \cdot s^2}) / \mathrm{m^8} \quad (4)$$

The fan's operating point is determined by the intersection point of the centrifugal fan's external characteristic curve and the ventilation system's wind resistance curve. With the radial air duct width of 80 mm and the radial blade width of 650 mm as the initial self-circulating hydrogen-cooled structure dimensions, the open-circuit static pressure, short-circuit hydrogen flow rate, and effective hydrogen flow rate of the generator can be obtained from the models [22]:

$$p_0 = \eta_0 \rho \left(u_2^2 - u_1^2\right) \quad (5)$$

$$Q_0 = 0.42 \pi K u_2 D_2 b \quad (6)$$

$$Q = \sqrt{\frac{p_0 Q_0}{P_0 + Z_{total} Q_0^2}} = 5.51\ \mathrm{m^3 / s} \quad (7)$$

Based on the equations, the aerodynamic efficiency of the fan blade is described, and the fan adopts radial blades with η_0=0.6. In the equations, u_1 and u_2 are the linear velocity of the inner and outer edges of the radial blade, m/s; K is the blade coefficient; D_2 is the diameter of the outer edge of the fan blade, m; b is the width of the fan blade, m; Z_{total} is the total wind resistance of the ventilation system. According to the results of the analytical analysis, the self-circulation system can provide about 5.51 m^3/s of cooling hydrogen flow rate to ensure overall cooling performance.

B. The Influence of the Cooling Gas Type on the Temperature Rise of the Generator

The cooling fluid used in the generator requires good insulation and thermal conductivity, and the commonly used cooling fluids are air and hydrogen. In this paper, the influences of the two fluids are compared with the enclosed self-circulating cooling system, and the heat dissipation characteristics are investigated.

To analyze the cooling capacities of the system with hydrogen and air as the coolants, the temperature field distribution of the windings and PMs of the PM wind generator was obtained by replacing the cooling medium with hydrogen under the enclosed self-circulating air cooling structure. Figs. 9 to 12 show that the maximum temperature rise of the winding and PM is 104.50 K and 78.23 K when uses air as the coolant. The maximum temperature rise of the winding and PM reduce to 89.71 K and 66.74 K when cooled by hydrogen. Compared to air cooling, the maximum temperature rise of the windings is reduced by 14.79 K and that of the PM by 11.49 K. It shows that hydrogen has a better cooling effect on the generator. In addition, due to the significant difference in its density and viscosity coefficient and the unevenness of axial wind speed distribution, the position of the maximum temperature rise of the winding and PM also changes.

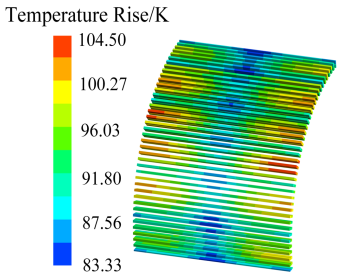

Fig. 9. Winding temperature rise under air cooled structure.

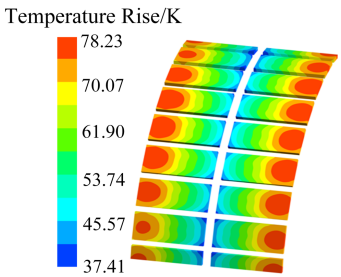

Fig. 10. Temperature rise of PM in air cooled structure.

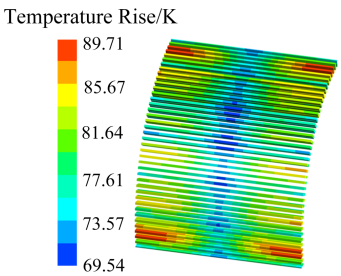

Fig. 11. Winding temperature rise under hydrogen cooled structure.

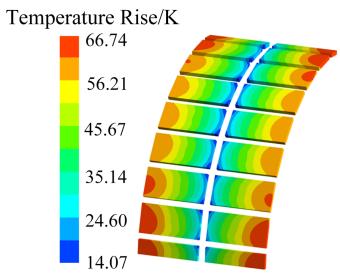

Fig. 12. Temperature rise of PM in hydrogen cooled structure.

V. Optimization of Hydrogen Cooling System Based on Taguchi

A. The Value of the Variable in the Taguchi Method

The Taguchi method is an optimization method based on the design of the experiment (DOE), which realizes the decoupling analysis of the influencing factors of each variable with less orthogonal design scheme combination by

establishing an orthogonal experiment table. In the study of this paper, four optimization variables are selected: axial ventilation channel width *w*, axial ventilation channel height *h*, axial ventilation channel number *m*, and radial air duct width *d*. Table IV shows the variable value levels, with the highest temperature of the winding rising T_W and the highest T_{PM} of the PM as the optimization goals.

TABLE IV
OPTIMIZATION PARAMETERS AND FACTOR LEVEL CONFIGURATION TABLE

Parameter level	*w*	*h*	*m*	*d*
I	180	25	4	40
II	200	32.5	5	50
III	220	40	6	60

B. Experimental Design of the Taguchi Method

According to the number and level of optimization variables, the standard orthogonal table L9(3^4) is established, as shown in Table V. According to Table V, the generator temperature rise calculation model was established, and the maximum temperature rise T_W of windings and T_{PM} of PM were calculated.

TABLE V
ORTHOGONAL EXPERIMENT TABLE

Serial number	*w*	*h*	*m*	*d*	T_{PM}/K	T_W/K
1	II	II	II	II	62.09	86.31
2	II	I	I	I	69.03	94.73
3	II	III	III	III	61.98	84.13
4	I	II	I	III	66.57	85.62
5	I	I	III	II	59.31	85.05
6	I	III	II	I	65.63	88.32
7	III	II	III	I	68.02	91.43
8	III	I	II	III	62.95	82.50
9	III	III	I	II	62.34	87.37

C. Simulation Data Analysis

Firstly, the averaged value of the optimization target under each level of each variable was calculated to analyze the temperature rise variance with respect to the level of each optimization variable. The variations of T_{PM} and T_W at different value levels of each optimization variable are shown in Fig. 13 and Fig. 14.

$$m_{T_{ij}} = \sum_{e_{Kj}=i} T_K / 3 \tag{8}$$

$$m_{W_{ij}} = \left(\sum_{e_{Kj}=i} w_K \right) / 3 \tag{9}$$

where $m_{T_{ij}}$ is the average temperature rise of the PM at level *i*, $m_{W_{ij}}$ is the average temperature rise of the winding of variable *j* at level *i*, and e_{Ki} is the level of the calculated variable *j* at layer *K*. T_K is the estimated temperature rise in layer *K*.

Calculate the variance of the two optimization objectives on the optimization variables and analyze the influence of each factor on the optimization objectives:

$$S_A = \frac{1}{3}\sum_{j=1}^{3}\left(m_{A_{(j)}} - m\right)^2 \tag{10}$$

where $m_{A_{(j)}}$ is the average temperature rise of variable A at level *j*, as shown in Table VI. According to the variance calculation results listed in Table VI and the optimization objectives illustrated in Figs. 13 and 14, the values of each influencing variable are determined, as tabulated in Table VII.

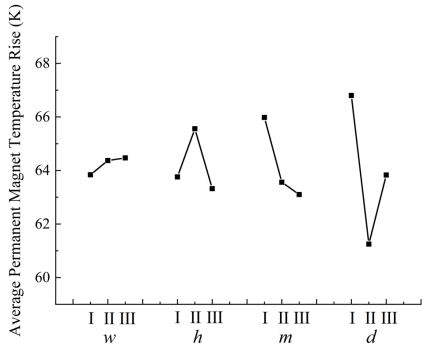

Fig. 13. Influence of each optimization variable on T_{PM}.

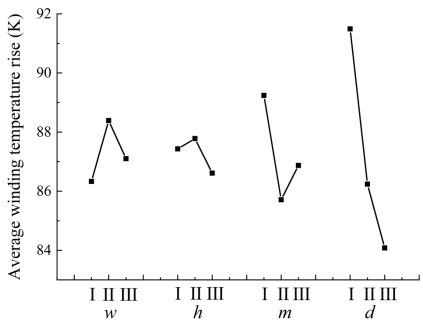

Fig. 14. Influence of each optimization variable on T_W.

TABLE VI
VARIANCE TABLE

Variable	*w*	*h*	*m*	*d*
S_T	0.072	0.94	1.8	6.71
S_W	0.73	0.24	2.15	9.69

TABLE VII
VALUES OF EACH INFLUENCE VARIABLE

Variable	*w*	*h*	*m*	*d*
Level	I	III	III	III
Valid values	180 mm	40 mm	6	60 mm

The fluid-thermal coupled fields of the generator with the optimized variable combinations are simulated, as shown in Figs. 15 and 16. The maximum temperature rises of the winding and the PMs are 79.11 K and 57.08 K, respectively. Through the design optimization of the hydrogen cooling system based on the Taguchi method, the maximum temperature rises of the winding and the PMs are further reduced by 10.60 K and 9.66 K, respectively.

Table VIII compares the temperature rises of the windings and the PMs with different cooling structures. *A*, *B*, *C*, and *D* represent the forced air cooling, self-circulating air cooling, self-circulating hydrogen cooling, and hydrogen-cooled cooling structure optimized by the Taguchi method, respectively.

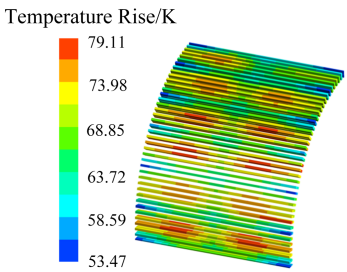

Fig. 15. Winding temperature rise distribution.

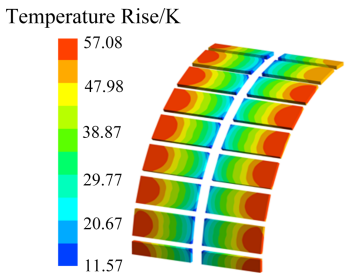

Fig. 16. Temperature rise distribution of PM。

TABLE VIII
TEMPERATURE RISE VALUES OF T_W AND T_{PM} UNDER DIFFERENT COOLING STRUCTURES

Cooling structure	*A*	*B*	*C*	*D*
T_{PM}/K	60.40	78.23	66.74	57.08
T_W/K	72.53	104.50	89.71	78.23

VI. CONCLUSION

This paper proposes an enclosed self-circulating hydrogen cooling system for a 1.65 MW direct-drive PM wind generator with the rotor panel supports working as the radial blades. The cooling hydrogen is driven by the centrifugal blades rotating synchronously in the central area and flows through the radial and axial dust to realize the efficient heat dissipation of the generator. The CFD numerical calculation results prove the effectiveness of the proposed cooling structure, as the temperature rise of the PM generator can be maintained at 89.71 K. To further improve the heat dissipation capacity, the cooling structural parameters are optimized based on the Taguchi method. The results show that the winding and PM temperature rises can be reduced by 11.48 K and 9.66 K, respectively, with the optimal combination of the cooling structural parameters.

REFERENCES

[1] B. Liu, Z. J. He, and H. Jin, "Wind Power Status and Development Trends," *Journal of Northeast Dianli University*, vol. 36, no. 2, pp. 7–13, Apr. 2016.

[2] M. L. Wymore, J. E. V. Dam, and H. Ceylan *et al,* "A Survey of Health Monitoring Systems for Wind Turbines," *Renewable and Sustainable Energy Reviews*, vol. 52, pp. 976–990, Dec. 2015.

[3] F. X. Wang, "Application and Development Tendency of PM Machines in Wind Power Generation System," *Transactions of China Electrotechnical Society*, vol. 27, no. 3, pp. 12–24, Mar. 2012.

[4] Z. D. Yuan, S. F. Jia, and D. L. Liang *et al*, "Research on Slot-pole Combination in High-power Direct-drive PM Vernier Generator for Fractional Frequency Transmission System," *CES Transactions on Electrical Machines and Systems*, vol. 6, no. 4, pp. 445–453, Dec. 2022.

[5] L. F. Zhu, T. L. Zhu, and Y. S. Bo *et al*, "Analytical Approach for Calculation of Eddy Current Losses in Magnets Caused by Permeance Harmonics in Air Gap," *Electric Machines and Control*, vol. 24, no. 5, pp. 10–16+25, Jun. 2020.

[6] G. H. Du, W. X, and J. G. Zhu *et al*, "Power Loss and Thermal Analysis for High-power High-speed Permanent Magnet Machines," *IEEE Transactions on Industrial Electronics*, vol. 67, no. 4, pp. 2722–2733, Apr. 2020.

[7] G. H. Du, T. Pu, and Q. X. Zhou *et al*, "Multiphysics Comparative Study of High Speed PM Machines for Ring PM Rotor and Solid PM Rotor," *IEEE Transactions on Energy Conversion*, vol. 38, no. 2, pp. 1421–1432, Jun. 2023.

[8] S. Y. Ding, L. J. Miao, and D. G. Xu *et al*, "Investigation of Heat Transfer Characteristic Inside 3 MW Permanent Magnet Wind Generator," *Large Electric Machine and Hydraulic Turbine*, vol. 222, no. 3, pp. 1–4+12, May. 2012.

[9] Y. Wu, Z. F. Zhang, and J. Q. Ping, "New Type Water Cooling Structure Design and Temperature Field Analysis of High Power Density Axial Flux Permanent Magnet Motor," *Proceedings of the CSEE*, vol. 41, no. 24, pp. 8295–8305, Dec. 2021.

[10] M. C. Jing, and J. C. Liu, "Design and Analysis of Cooling System for Megawatt Modular Permanent Magnet Wind Turbine Generator Stator," *Thermal Power Generation*, vol. 51, no. 2, pp. 171–177, Nov. 2022.

[11] S. Y. Ding, B. C. Guo, and Z. Q. Sun, "Ventilation Structure Optimization and Performance Analyses of Permanent Magnet Wind Generators," *Proceedings of the CSEE*, vol. 33, no. 9, pp. 122–128, Mar. 2013.

[12] X. G. Fan, R. H. Qu, and J. Li *et al*, "Ventilation and Thermal Improvement of Radial Forced Air-cooled FSCW Permanent Magnet Synchronous Wind Generators," *IEEE Transactions on Industry Applications*, vol. 53, no. 4, pp. 3447–3456, Jul.-Aug. 2017.

[13] M. Polikarpova, P. Ponomarev, and P. Roytta *et al*, "Direct Liquid Cooling for an Outer-rotor Direct-drive Permanent-magnet Synchronous Generator for Wind Farm Applications," *IET Electric Power Applications*, vol. 9, no. 8, pp. 523–532, Sept. 2015.

[14] Y. Su, W. L. Li, and W. M. Li *et al*, "Heat Transfer Coefficient Distribution in Inner Surface of Stator Ventilation Duct for Large Capacity Air-cooled Turbine Generator," *Journal of Thermal Analysis and Calorimetry*, vol. 146, no. 5, pp. 2279–2289, Nov. 2020.

[15] S. Y. Ding, and C. C. Wu, "Characteristics of Fluid Flow and Heat Transfer for a 5 Megawatt Wind Generator with Radial Ventilation Structure," *Electric Machines and Control*, vol. 23, no. 10, pp. 68–76, Oct. 2019.

[16] X. F. Wang, Y. Dai, and J. Luo, "Waterway Design and Temperature Field Analysis of Vehicle Permanent Magnet Synchronous Motor Based on Fluid-solid Coupling," *Transactions of China Electrotechnical Society*, vol. 34, no. zk1, pp. 22–29, Jul. 2019.

[17] S. Y. Ding, M. Zhu, and X. Jiang, "Coupling Study of 3D Universal Temperature Field and Temperature Stress for Permanent Magnet Synchronous Motor," *Electric Machines and Control*, vol. 22, no. 1, pp. 53–60+71, Jan. 2018.

[18] G. J. Zhu, Y. H. Zhu, and W. M. Tong *et al*, "Double-circulatory Thermal Analyses of a Water-cooled Permanent Magnet Motor Based on a Modified Model," *IEEE Transactions on Magnetics*, vol. 54, no. 3, pp. 1–4, Mar. 2018.

[19] J. C. Zhang, and B. J. Ge, "Design and Thermal Performance Analysis of a New Water-cooled Structure for Permanent Magnet Synchronous Motors for Electric Vehicles," *Thermal Science*, vol. 27, no. 3B, pp. 2423–2432, Sept. 2023.

[20] L. K. Wang, Y. Li, and B. Q. Kou *et al*, "Influence of Ventilation Modes on the 3D Global Heat Transfer of PMSM Based on Polyhedral Mesh," *IEEE Transactions on Energy Conversion*, vol. 37, no. 2, pp. 1455–1466, Jun. 2022.

[21] L. N. Li, N. Jia, and X. Z. Wang *et al*, "Cooling System Design Optimization of an Enclosed PM Traction Motor for Subway Propulsion Systems," *CES Transactions on Electrical Machines and Systems*, vol. 7, no. 4, pp. 390–396, Dec. 2023.

[22] G. J. Zhu, X. M. Liu, and L. N. Li *et al*, "Design and Analysis of the Ventilation Structure for a Permanent Magnet Wind Generator,"

Transactions of China Electrotechnical Society, vol. 34, no. 5, pp. 946–953, Mar. 2019.

[23] G. J. Zhu, Y. H. Zhu, and W. M. Tong *et al*, "Analysis and Enhancement of Cooling System of High-speed Permanent Magnet Motor Based on Computational Fluid Dynamics," *Advanced Technology of Electrical Engineering and Energy*, vol. 36, no. 12, pp. 1–7, Dec. 2017.

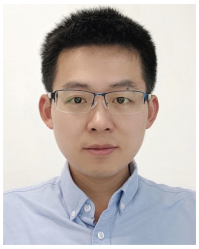

Gaojia Zhu (Member, IEEE) received his Ph.D. degree in Electrical Engineering from the National Engineering Research Center for Rare-Earth Permanent Magnet Machines, Shenyang University of Technology, Shenyang, China, in 2017. He is currently an associate professor with the School of Electrical Engineering, Tiangong University, Tianjin, China. He has been a postdoctoral visiting researcher with the Power Electronics, Machines, and Control Research Group, University of Nottingham, Nottingham, U. K., from Dec. 2022 to Dec. 2023, and a visiting researcher with The Hong Kong Polytechnic University from July to Aug. 2018. His research interests include the multi-physical analysis and multi-disciplinary design optimization of PMSMs, transformers, and power modules.

YunHao Li received his B.S. degree in electrical engineering from Shijiazhuang University, Shijiazhuang, China, in 2020. He is currently pursuing his M.E. degree in electrical engineering with the School of Electrical Engineering, Tiangong University, Tianjin, China.

His research interest is the design and optimization of permanent magnet machines.

Longnv Li (Member, IEEE) received her Ph.D. degree in Electrical Engineering from the National Engineering Research Center for Rare-Earth Permanent Magnet Machines, Shenyang University of Technology, Shenyang, China, in 2016. She is currently an associate professor with the School of Electrical Engineering, Tiangong University, Tianjin, China. She has also been a visiting researcher with The Hong Kong Polytechnic University from Dec. 2013 to Nov. 2014, and July to Aug. 2018.

Her research interests are the multi-physics coupled analysis and optimal design of electrical machines, transformers, and power modules.